

# Collective Variable Free Transition Path Sampling with Generative Flow Network

Kiyoung Seong<sup>1</sup>Seonghyun Park<sup>1</sup>Seonghwan Kim<sup>2</sup>Woo Youn Kim<sup>2</sup>Sungsoo Ahn<sup>1</sup><sup>1</sup>POSTECH <sup>2</sup>KAIST{kyseong, shpark26, sungsoo.ahn}@postech.ac.kr,  
{dmdtka00, wooyoun}@kaist.ac.kr

## Abstract

Understanding transition paths between meta-stable states in molecular systems is fundamental for material design and drug discovery. However, sampling these paths via molecular dynamics simulations is computationally prohibitive due to the high-energy barriers between the meta-stable states. Recent machine learning approaches are often restricted to simple systems or rely on collective variables (CVs) extracted from expensive domain knowledge. In this work, we propose to leverage generative flow networks (GFlowNets) to sample transition paths without relying on CVs. We reformulate the problem as amortized energy-based sampling over molecular trajectories and train a bias potential by minimizing the squared log-ratio between the target distribution and the generator, derived from the flow matching objective of GFlowNets. Our evaluation on three proteins (Alanine Dipeptide, Polypeptide, and Chignolin) demonstrates that our approach, called TPS-GFN, generates more realistic and diverse transition paths than the previous CV-free machine learning approach.

## 1 Introduction

In material design and drug discovery, understanding the mechanisms and kinetics of transitions between meta-stable states of molecular systems, such as protein folding and chemical reactions [1, 2, 3, 4], is crucial. A comprehensive study of them requires sampling diverse transition paths [5, 6], which provide insights into mechanisms and energy landscapes. However, sampling transition paths through unbiased molecular dynamics (MD) simulations is challenging due to the high-energy barriers of intermediate states, which cause an exponential decay in transition probability [7]. Thus, a brute-force search through unbiased MD simulations is impractical within a realistic computational budget.

To address this problem, researchers have developed bias potential enhanced sampling (BPES) methods such as umbrella sampling [8], meta-dynamics [9], and adaptive biasing force [10, ABF] methods. BPES methods rely on auxiliary *bias potentials* (or *forces*) to facilitate transitions across high-energy barriers. These methods design bias potentials using collective variables (CVs), functions of atomic coordinates that capture the slow modes of the transition. While effective for some systems, the reliance on expensive domain knowledge limits the applicability of BPES methods to systems where CVs are less understood.

Recently, machine learning has emerged as a promising paradigm for designing bias potentials (or forces) without relying on CVs [11, 12, 13, 14]. For instance, Das et al. [11] and Lelièvre et al.

Project page: [https://anonymous.4open.science/w/tps\\_gflow/](https://anonymous.4open.science/w/tps_gflow/).



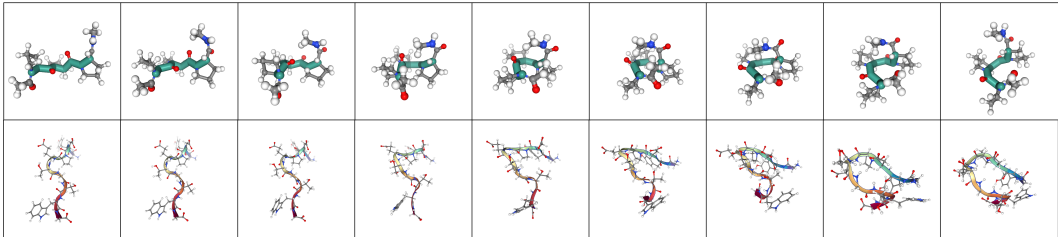


Figure 1: Visualization of transition paths generated by our TPS-GFN, progressing from left to right over time. **(Top)** Polyproline transformation from the meta-stable region PP-II to PP-I. **(Bottom)** Chignolin folding process.

[12] used reinforcement learning to sample transition paths from biased molecular dynamics with a parametrized force that approximates the transition path distribution. However, these works are limited to two-dimensional systems. Holdijk et al. [14] trained the bias potential by minimizing KL divergence on the trajectories collected by itself, i.e., on-policy training. Still, this approach suffers from mode-seeking behavior, and the on-policy training does not reuse the collected trajectories, leading to inefficiency in sample complexity.

**Contribution.** In this work, we propose TPS-GFN, generative flow networks [15, GFlowNets] (GFN) for transition path sampling (TPS), which trains the bias potential without requiring collective variables (CVs). To this end, we formulate the problem as the energy-based sampling over molecular trajectories between the given meta-stable states. GFlowNet allows off-policy training and avoids collapsing to a particular mode of distribution over transition paths.

In particular, our method trains the bias potential by minimizing the squared log-ratio between the target distribution and the generator, which we derive from the one-step trajectory balance (TB) objective [16, 17]. We use a replay buffer to store the molecular trajectories, which are later used for off-policy training of the generator. Furthermore, we also design a new reward function to provide dense training signals and evaluate molecular trajectories with various lengths between the meta-stable states.

We extensively evaluate our method for three peptides, i.e., Alanine Dipeptide, Polyproline, and Chignolin. We demonstrate that our method faithfully generates a realistic transition path between the given meta-stable states in Figure 1, outperforming the prior ML-based approach [14]. We also show that our method discovers diverse transition states.

## 2 Related work

### 2.1 Collective variable-based transition path sampling

**Bias potential methods.** Bias potential (or force) was originally introduced in enhanced sampling to explore molecular conformations that are difficult to access by the unbiased molecular dynamics (MD) within limited simulation times [18]. We focus on adaptive bias simulations such as meta-dynamics [9] and adaptive biasing force (ABF) [10], which updates the bias potential (or force) adaptively. Meta-dynamics and ABF add bias potential (or force) in a time-dependent manner and enhance the sampling along a few well-designed collective variables (CVs). Other methods for sampling transition paths using bias potentials (or forces) include the umbrella sampling [8], and the Wang-Landau method [19].

**MCMC-based methods.** Shooting is a well-established method using the Markov chain Monte Carlo (MCMC) procedure on path space [20]. To be specific, it perturbs a shooting point in the transition path, performs MD simulations from it, and proposes new paths. Borrero et al. [21] perturbed the shooting point with meta-dynamics to avoid traps in path space, and Jung et al. [22] trained the parameterized commitor function to select the shooting point with a high acceptance rate. Plainer et al. [23] used latent proposals to leverage information from the latent space of the Boltzmann generator. However, the MCMC-based method suffers from long mixing times to sample independent transition paths, and there is a trade-off between the acceptance rate and diversity. Falkner et al. [24]



generated independent shooting points from the Boltzmann generator using the bias potential with the umbrella sampling, but this method relies on CVs and shooting region.

**Automated learning of CV.** Since many algorithms rely on CVs which require expensive domain knowledge about transitions, researchers have explored automating the derivation of CV from data [25, 26, 27, 28]. Bonati et al. [25] and Trizio et al. [26] used time-lagged independent component analysis and applied deep linear discriminant analysis on MD trajectories. Ray et al. [27] and Yang et al. [28] considered the transition path ensemble as effective data augmentation strategies for discriminant analysis to discover CVs, respectively.

## 2.2 Collective variable-free transition path sampling

**Generation from a fixed dataset.** Given a dataset of transition paths, one can train generative models using the dataset to sample a transition path. Petersen et al. [13] and Lelièvre et al. [12] applied diffusion probabilistic models and [29] variational auto-encoders [30], respectively. However, these methods are limited to small systems, as collecting the transition paths is notoriously difficult due to high energy barriers.

**Bias potential-based method.** Without any previously collected dataset of transition paths, Das et al. [11] and Hua et al. [31] considered transition path sampling as a reinforcement learning (RL) problem and trained the bias potentials (or forces) of the policy by minimizing KL divergence. However, these works are limited to 2-dimensional systems. Notably, Holdijk et al. [14] applied the path integral cross-entropy [32] used in stochastic optimal control framework to scale up to larger systems.

## 2.3 Generative flow networks

Generative flow networks (GFlowNets) are the learning framework for amortized inference, generating objects through a series of decisions with a stochastic policy, or forward policy. [15, 16]. By learning the policy to sample an object proportionally to their rewards, GFlowNets can produce diverse samples [15]. To be specific, they train the forward policy by matching its trajectory flow with an auxiliary backward trajectory flow. Training objectives such as flow matching [15], trajectory balance [17], and detailed balance [16] have been proposed. Recent studies have successfully applied GFlowNets to tasks including molecular conformer generation [33], drug discovery [34], crystal structure design [35], and biological sequence design [36].

**Comparison with RL and variational inference.** RL and variational inference algorithms share similarities with GFlowNets in learning a target distribution specified by a reward function. GFlowNets and RL both make sequential decisions to achieve high rewards, but GFlowNets differ by sampling proportionally to the reward rather than maximizing it. Moreover, while variational inference algorithms aim to learn the target (Boltzmann) distribution, GFlowNets reduce gradient variance by estimating marginal quantities and allow off-policy learning without the need for reweighted importance sampling [37].

# 3 Method

## 3.1 Problem setup

At a high level, our goal is to sample transition paths from one meta-stable state to another meta-stable state through unbiased molecular dynamics (MD), e.g., transition paths from the meta-stable region  $C5$  to  $C7_{ax}$  in Alanine Dipeptide, as illustrated in Figure 2. However, since such events occur rarely in naïve MD simulation. To this end, we aim to train a neural network to search for such transition paths.

**Molecular dynamics.** We consider MD simulations that describe motion of a molecular state  $\mathbf{x} = (\mathbf{r}, \mathbf{v})$  with  $N$  atoms, given the atom-wise positions (or conformation)  $\mathbf{r} \in \mathbb{R}^{N \times 3}$  and the

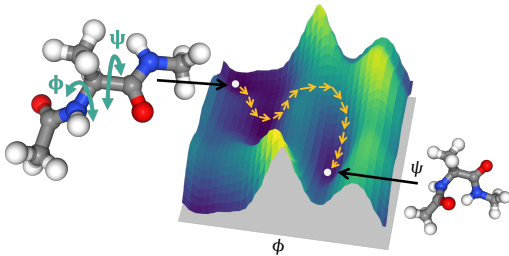


Figure 2: The potential energy landscape of Alanine Dipeptide with its collective variable (CV), i.e., two dihedral angles ( $\phi, \psi$ ). We aim to generate a transition path from one meta-stable state to another, highlighted with yellow arrows.



atom-wise velocities  $\mathbf{v} \in \mathbb{R}^{N \times 3}$ . In particular, we consider Langevin dynamics [38] to describe the molecular motion:

$$d\mathbf{r} = \mathbf{v}dt, \quad d\mathbf{v} = \frac{-\nabla_{\mathbf{r}}U(\mathbf{r})}{m}dt - \gamma\mathbf{v}dt + \sqrt{\frac{2\gamma k_B \lambda}{m}}d\mathbf{w},$$

where  $U(\mathbf{r})$ ,  $m$ ,  $\gamma$ ,  $k_B$ ,  $\lambda$ , and  $d\mathbf{w}$  denote the potential energy, atom-wise masses, the friction term, Boltzmann constant, temperature, and the Brownian motion, respectively.

**Euler Maruyama discretization.** Langevin dynamics can be discretized into a sequence of molecular states  $\mathbf{x}_0, \mathbf{x}_1, \dots, \mathbf{x}_T$  using the Euler Maruyama method [39] as follows:

$$\mathbf{r}_t = \mathbf{r}_{t-1} + \mathbf{v}_{t-1}\Delta, \quad \mathbf{v}_t = (1 - \gamma\Delta)\mathbf{v}_{t-1} - \frac{\nabla_{\mathbf{r}}U(\mathbf{r}_t)}{m}\Delta + \sqrt{\frac{2\gamma k_B \lambda}{m}}\boldsymbol{\varepsilon}_t\Delta,$$

where  $\Delta$  is the discretization step size and  $\boldsymbol{\varepsilon}_t \in \mathbb{R}^{N \times 3}$  is a noise from the standard normal distribution. We denote the conditional probabilities described by this discretization as  $p_{\text{MD}}(\mathbf{x}_t|\mathbf{x}_{t-1})$ .

**Transition path sampling.** One of the challenges in sampling transition paths through unbiased MD simulations is the meta-stability: a state can remain trapped for a long time in the initial meta-stable region  $\mathcal{A} \subseteq \mathbb{R}^{N \times 3}$  before transitioning into a distinct meta-stable region  $\mathcal{B} \subseteq \mathbb{R}^{N \times 3}$ . Our goal is to sample a transition path  $\mathbf{x}_{0:T} = (\mathbf{x}_0, \dots, \mathbf{x}_T)$  that links the distinct regions  $\mathcal{A}$  and  $\mathcal{B}$  where  $\mathbf{r}_0 \in \mathcal{A}$ ,  $\mathbf{r}_T \in \mathcal{B}$  and  $T$  is the length of the trajectory.

Since the meta-stable region  $\mathcal{A}$  and  $\mathcal{B}$  are not well-specified for many molecular systems, we find unique local minima  $\mathbf{r}_{\mathcal{A}}$  and  $\mathbf{r}_{\mathcal{B}}$  of the potential function inside the meta-stable regions  $\mathcal{A}$  and  $\mathcal{B}$ , respectively. Afterwards, we sample a transition path  $\mathbf{x}_{0:T}$  that starts from the state  $\mathbf{x}_0 = \mathbf{x}_{\mathcal{A}}$  and ends nearby the conformation  $\mathbf{r}_{\mathcal{B}}$ , i.e.,  $\mathbf{r}_T \in \mathcal{B}$ . To be specific, we fix  $\mathbf{x}_0 = \mathbf{x}_{\mathcal{A}}$  and sample the remaining trajectory  $\mathbf{x}_{1:T}$  from the following distribution:

$$p_{\mathcal{A},\mathcal{B}}(\mathbf{x}_{1:T}|\mathbf{x}_0) = \frac{1}{Z} \mathbf{1}_{\mathcal{B}}(\mathbf{r}_T) \prod_{t=1}^T p_{\text{MD}}(\mathbf{x}_t|\mathbf{x}_{t-1}) \quad (1)$$

where  $Z$  is the normalizing constant and  $\mathbf{1}_{\mathcal{B}}(\mathbf{r}_T)$  is the binary indicator function for the final conformation  $\mathbf{r}_T$  being in the meta-stable region  $\mathcal{B}$ . In other words,  $\mathbf{1}_{\mathcal{B}}(\mathbf{r}_T) = 1$  if  $\mathbf{r}_T \in \mathcal{B}$ , and  $\mathbf{1}_{\mathcal{B}}(\mathbf{r}_T) = 0$  otherwise.

To sample transition paths from the target distribution  $p_{\mathcal{A},\mathcal{B}}(\mathbf{x}_{1:T}|\mathbf{x}_0)$ , one can use rejection sampling. This involves sampling  $\mathbf{x}_{1:T}$  through unbiased MD simulations and then checking if  $\mathbf{r}_T \in \mathcal{B}$ . However, this method is computationally expensive due to the low acceptance rate, which is caused by the high-energy barriers.

### 3.2 TPS-GFN: GFlowNets for transition path sampling

In this section, we explain our approach, called TPS-GFN, that amortizes the expensive cost of sampling transition paths from the distribution  $p_{\mathcal{A},\mathcal{B}}(\mathbf{x}_{1:T}|\mathbf{x}_0)$ . Our key idea is threefold: (1) using the trajectory balance (TB) objective to train a generator  $p_{\theta}(\mathbf{x}_{1:T}|\mathbf{x}_0) = \prod_{t=1}^T p_{\theta}(\mathbf{x}_t|\mathbf{x}_{t-1})$  towards the true distribution  $p_{\mathcal{A},\mathcal{B}}(\mathbf{x}_{1:T}|\mathbf{x}_0)$ , (2) relaxation of the target distribution, and (3) parameterization of the generator with the bias potential. We provide a full description of the algorithm in [Algorithm 1](#).

**Training with trajectory balance (TB).** We aim to make the generator  $p_{\theta}(\mathbf{x}_{1:T}|\mathbf{x}_0)$  imitate the target distribution  $p_{\mathcal{A},\mathcal{B}}(\mathbf{x}_{1:T}|\mathbf{x}_0)$ . From [Equation \(1\)](#), we can achieve this by satisfying the following identity:

$$\left( \log \frac{Z \prod_{t=1}^T p_{\theta}(\mathbf{x}_t|\mathbf{x}_{t-1})}{\mathbf{1}_{\mathcal{B}}(\mathbf{r}_T) \prod_{t=1}^T p_{\text{MD}}(\mathbf{x}_t|\mathbf{x}_{t-1})} \right)^2 = 0,$$

for all trajectories  $\mathbf{x}_{1:T}$ . To this end, we propose to use the one-step TB objective [17], the squared log-ratio between the unnormalized generator  $Z_{\theta}p_{\theta}(\mathbf{x}_{1:T}|\mathbf{x}_0)$  and the unnormalized target distribution  $\mathbf{1}_{\mathcal{B}}(\mathbf{r}_T) \prod_{t=1}^T p_{\text{MD}}(\mathbf{x}_t|\mathbf{x}_{t-1})$ , as follows:

$$\mathcal{L}_{\text{TB}}(\mathbf{x}_{1:T}; \theta) = \left( \log \frac{Z_{\theta} \prod_{t=1}^T p_{\theta}(\mathbf{x}_t|\mathbf{x}_{t-1})}{\mathbf{1}_{\mathcal{B}}(\mathbf{r}_T) \prod_{t=1}^T p_{\text{MD}}(\mathbf{x}_t|\mathbf{x}_{t-1})} \right)^2, \quad (2)$$



---

**Algorithm 1** GFlowNet training for transition path sampling

---

- 1: Initialize an empty replay buffer  $\mathcal{B}$ , the biased potential  $b_\theta(\mathbf{r})$ , and the parameter  $Z_\theta$ .
  - 2: **for**  $i = 1, \dots, I$  **do**
  - 3:   Sample  $M_1$  trajectories  $\{\mathbf{x}_{0:T}^{(m)}\}_{m=1}^{M_1}$  from the tempered version of biased MD (Equation (3)).
  - 4:   Update the replay buffer  $\mathcal{B} \leftarrow \mathcal{B} \cup \{\mathbf{x}_{0:T}^{(m)}\}_{m=1}^{M_1}$ .
  - 5:   **for**  $j = 1, \dots, J$  **do**
  - 6:     Sample  $M_2$  paths  $\{\mathbf{x}_{0:T}^{(m)}\}_{m=1}^{M_2}$  from the replay buffer  $\mathcal{B}$ .
  - 7:     Update parameters  $\theta$  to minimize the loss  $\mathcal{L}$  (Equation (2)) using the samples  $\{\mathbf{x}_{0:T}^{(m)}\}_{m=1}^{M_2}$ .
  - 8:   **end for**
  - 9: **end for**
- 

where  $Z_\theta \in \mathbb{R}$  is a learnable scalar parameter to estimate the normalization constant  $Z$ . We match the generator with the target distribution by minimizing the loss function  $\mathcal{L}_{\text{TB}}(\mathbf{x}_{1:T}; \theta)$  over trajectories  $\mathbf{x}_{1:T}$  sampled from an *arbitrary* training distribution, i.e., off-policy training. We provide an explicit derivation of the one-step TB objective (Equation (2)) in Appendix A.

To leverage the ability of the TB objective, we use a replay buffer that collects the past samples from the tempered version of the generator and reuses them for training. This improves sample efficiency and stability of training, both for GFlowNets [15] and reinforcement learning [40]. TPS-GFN alternates between (1) sampling from the generator to store molecular trajectories in the replay buffer and (2) training the generator on samples from the replay buffer, as described in Algorithm 1.

As shown by Malkin et al. [37], the TB objective automatically performs gradient variance reduction for variational inference by estimating a marginal quantity (the partition function) that acts as a baseline and allows off-policy learning without the need for reweighted importance sampling. This is also a slight modification to the VarGrad objective [41, 42] that was proposed to reduce the gradient of evidence lower bound (ELBO).

We note the similarity of our TPS-GFN with the prior work [14], which minimizes the Kullback-Leibler (KL) divergence between the generator and the target distribution. In comparison, the TB objective yields better training dynamics due to reduced variance in the gradients, and better sample efficiency due to the ability to reuse the collected sample with an external replay buffer. Furthermore, TPS-GFN does not suffer from the mode-seeking behavior of KL divergence.

**Target distribution relaxation.** Learning to imitate the target distribution  $p_{\mathcal{A}, \mathcal{B}}$  with TB objective is challenging since its probability is rarely non-zero. To alleviate this issue, we relax the target distribution by (1) allowing trajectories to reach the meta-stable region  $\mathcal{B}$  before termination and (2) relaxing the binary indicator function into a smooth function. In particular, we relax the target distribution into the following form:

$$\tilde{p}_{\mathcal{A}, \mathcal{B}}(\mathbf{x}_{1:T} | \mathbf{x}_0) = \frac{1}{\tilde{Z}} \tilde{\mathbf{1}}_{\mathcal{B}}(\mathbf{r}_{1:T}) \prod_{t=1}^T p_{\text{MD}}(\mathbf{x}_t | \mathbf{x}_{t-1}),$$

where  $\tilde{Z}$  is the normalizing constant and  $\tilde{\mathbf{1}}_{\mathcal{B}}(\mathbf{r}_{1:T})$  is the relaxed indicator function defined as follows:

$$\tilde{\mathbf{1}}_{\mathcal{B}}(\mathbf{r}_{1:T}) = \max_{t \in \{1, \dots, T\}} \exp \left( -\frac{\|D(\mathbf{r}_t) - D(\mathbf{r}_{\mathcal{B}})\|_F^2}{2\sigma^2} \right).$$

Here,  $\|\cdot\|_F$  is the Frobenius norm,  $\sigma > 0$  is a hyperparameter to control the degree of relaxation, and  $D(\mathbf{r}) \in \mathbb{R}^{N \times N}$  is a distance matrix with  $(i, j)$ -th element denoting the Euclidean distance  $\|\mathbf{r}_i - \mathbf{r}_j\|_2$  between the  $i$ -th and the  $j$ -th atoms [43].

**Parameterizing generator with bias potential.** Similar to Holdijk et al. [14], we model the generator  $p_\theta(\mathbf{x}_{1:T} | \mathbf{x}_0)$  as the discretization of the following biased Langevin dynamics:

$$d\mathbf{r} = \mathbf{v}dt, \quad d\mathbf{v} = -\frac{\nabla_{\mathbf{r}}(U(\mathbf{r}) + b_\theta(\mathbf{r}))}{m}dt - \gamma\mathbf{v}dt + \sqrt{\frac{2\gamma k_B \lambda}{m}}d\mathbf{w},$$

where  $b_\theta(\mathbf{r})$  is the bias potential that guides the Langevin dynamics towards the meta-stable region  $\mathcal{B}$ . We discretize the biased Langevin dynamics as follows:

$$\mathbf{r}_{t+1} = \mathbf{r}_t + \mathbf{v}_t \Delta, \quad \mathbf{v}_{t+1} = (1 - \gamma\Delta)\mathbf{v}_t + \frac{-\nabla_{\mathbf{r}}(U(\mathbf{r}_t) + b_\theta(\mathbf{r}_t))}{m}\Delta + \sqrt{\frac{2\gamma k_B \lambda}{m}}\boldsymbol{\varepsilon}_t \Delta, \quad (3)$$



Table 1: Benchmark scores on Alanine Dipeptide which have well-known CVs. All metrics are averaged over 64 trajectories. ETP and EFP are reported only if the final state is in the target meta-stable state. The best values are highlighted in **bold** except for MD. Values from Holdijk et al. [14] are indicated by †. Methods using bias force and potential are denoted by (F) and (P), respectively.

Method	EPD (↓) nm × 10 <sup>-3</sup>	THP (↑) %	ETP (↓) kJmol <sup>-1</sup>	LL (↑) × 10 <sup>2</sup>	EPCD (↓) nm	EFP (↓) kJmol <sup>-1</sup>
MD (300K)	7.78 ± 0.61	0.00	—	5.02 ± 0.15	88.27 ± 5.65	—
MD (9000K)	7.26 ± 2.47	3.12	770.18 ± 151.85	-25.47 ± 4.91	101.82 ± 31.02	604.02 ± 136.73
PIPS (F)	2.06 ± 0.27	56.25	0.48 ± 10.31	4.49 ± 0.36	12.15 ± 3.49	-15.85 ± 11.21
PIPS (P)†	1.21 ± 0.31	63.50	-8.35 ± 8.04	—	—	—
<b>TPS-GFN (F)</b>	1.05 ± 0.11	<b>98.43</b>	<b>-18.13 ± 4.67</b>	<b>4.91 ± 0.16</b>	5.12 ± 2.67	<b>-45.58 ± 7.12</b>
<b>TPS-GFN (P)</b>	<b>1.02 ± 0.08</b>	<b>98.43</b>	-16.62 ± 5.1	4.85 ± 0.12	<b>4.91 ± 1.70</b>	-45.18 ± 6.88

Table 2: Benchmark scores on Polyproline and Chignolin. All metrics are averaged over 64 trajectories. The best values are highlighted in **bold** except for MD. ‡ indicates reproduced results from the prior work [14]. Methods using bias force and potential are denoted by (F) and (P), respectively.

Molecule	Method	EPD (↓) nm × 10 <sup>-3</sup>	LL (↑) × 10 <sup>2</sup>	EPCD (↓) nm
Polyproline	MD (300K)	18.83 ± 1.59	4.45 ± 0.57	82.43 ± 3.69
	PIPS (F)‡	29.13 ± 2.94	-215.82 ± 87.03	111.46 ± 4.86
	PIPS (P)‡	12.21 ± 1.77	-210.27 ± 96.11	76.90 ± 6.17
	<b>TPS-GFN (F)</b>	<b>7.94 ± 2.13</b>	-6.93 ± 0.98	<b>42.85 ± 8.00</b>
	<b>TPS-GFN (P)</b>	13.86 ± 1.08	<b>2.64 ± 0.52</b>	83.23 ± 4.59
Chignolin	MD (300K)	381.68 ± 48.74	10.11 ± 1.03	259.63 ± 12.58
	PIPS (F)‡	68.02 ± 20.63	-251.19 ± 63.00	188.56 ± 29.77
	PIPS (P)‡	68.87 ± 9.39	-241.22 ± 58.15	186.30 ± 11.79
	<b>TPS-GFN (F)</b>	53.34 ± 5.92	-40.02 ± 4.07	157.44 ± 6.92
	<b>TPS-GFN (P)</b>	<b>26.31 ± 1.81</b>	<b>-0.88 ± 1.42</b>	<b>101.43 ± 7.27</b>

We model the bias potential  $b_\theta(\mathbf{r})$  or directly bias force  $\mathbf{b}_\theta(\mathbf{r}) = \nabla_{\mathbf{r}} b_\theta(\mathbf{r})$  for the generator. We use a multi-layered perception (MLP) architecture to parameterize the bias potential or force.

## 4 Experiment

### 4.1 Molecular systems

In this section, we evaluate our TPS-GFN on three molecular systems, (1) Alanine Dipeptide, (2) Polyproline Helix, and (3) Chignolin. We run molecular dynamics (MD) simulations on a femtosecond (fs) scale to sample paths and evaluate them at the temperature of 300K, using the OpenMM library. We report more details about OpenMM and model configurations in [Appendix B.1](#) and [Appendix B.2](#), respectively.

**Alanine Dipeptide.** The Alanine Dipeptide is a small peptide consisting of two alanine residues linked by a peptide bond. Alanine Dipeptide has a well-known collective variable (CV), i.e., two dihedral angles ( $\phi, \psi$ ). We sample the transition paths from the meta-stable region  $C5$  to  $C7_{ax}$  for a 500 fs.

**Polyproline Helix and Chignolin.** In our experiments, the Polyproline Helix consists of 3 proline residues while the Chignolin consists of 10 amino acid residues. Their CVs and mechanisms are less understood than Alanine Dipeptide due to their complexity. We sample transition paths of Polyproline between the meta-stable region PP-II and PP-I for a 10000 fs, and Chignolin folding process for a 5000 fs. In training, we use the tempered version of biased MD simulations at a temperature of 600K.



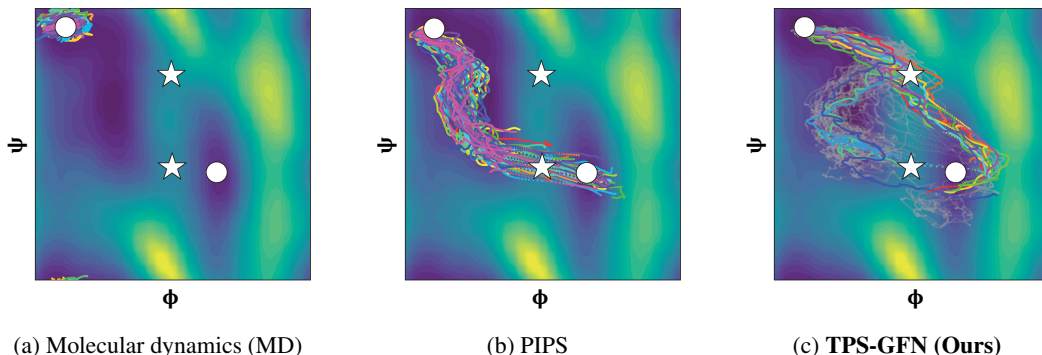


Figure 3: Visualization of 64 paths starting in meta-stable region  $C5$  on the Ramachandran plot of Alanine Dipeptide. White circles indicate meta-stable states, and stars indicate transition states. (a) The paths from unbiased MD simulations that fail to escape the initial meta-stable region. (b) The paths generated by PIPS, passing through only one transition state. (c) The paths generated by TPS-GFN, passing through both transition states. For clarity, 10 paths are highlighted.

## 4.2 Quantitative results

In our experiments, we compare our method with unbiased MD and PIPS [14]. To compare the generated transition paths, we consider three metrics following the prior work [14]. Expected pairwise distance (EPD) measures the similarity between the final conformation and the target conformation by comparing their interatomic distances. Similar to EPD, target hit percentage (THP) evaluates how many paths achieve the target meta-stable region in a binary manner. Unlike EPD and THP which only focus on the final conformation of the transition path, energy transition point (ETP) measures the maximum potential energy of a transition path, referring to the ability of a model to find the transition states when crossing the energy barrier.

However, ETP only evaluates the potential energy of a transition state, it can not reflect the reality of an overall transition path. To resolve this issue, we propose log-likelihood (LL) which refers to log-likelihood from the unbiased MD simulation. Similarly, since EPD and THP only consider the distance between the final conformation of sampled paths and the target conformation, they can not reflect the potential energy of the final conformation which explains its stability and reality. To evaluate it, we propose the potential energy of the final point (EFP), and the expected pairwise Coulomb distance (EPCD) which consider both the potential energy of the final conformation and the distance between the final conformation of sampled paths and the target conformation. EPCD measures both geometric and electrostatic similarity between the final conformation and the target conformation using the Coulomb matrix. The Coulomb matrix captures atomic mass and energy level around the final state better than the distance matrix. More details of metrics are in [Appendix B.3](#).

**Alanine Dipeptide.** Since Alanine Dipeptide has well-known CVs, i.e., two dihedral angles ( $\phi, \psi$ ), we can evaluate THP, ETP, and EFP which requires defining the meta-stable region with a CV. In [Table 1](#), our TPS-GFN outperforms the baselines for both previous metrics (EPD, THP, ETP) and proposed metrics (LL, EPCD, EFP) regardless of predicting bias potential or force. This shows that the TB objective used in our method leads to more realistic and high-quality transition paths than KL divergence used in PIPS. In particular, the 1.02 EPD and 98.43% THP score of TPS-GFN show that our method faithfully amortizes the rejection sampling from unbiased MD simulations. We also highlight that the EFP of our method is much closer to the potential energy of the target conformation  $r_{C7_{ax}}$ ,  $-84.86 \text{ kJmol}^{-1}$ , than the baselines.

**Polyproline Helix and Chignolin.** Unlike Alanine Dipeptide, the CVs of Polyproline Helix, and Chignolin are less understood. Therefore, we exclude metrics THP, ETP, and EFP which require CVs to define the meta-stable state. In [Table 2](#), our method consistently outperforms baselines in both Polyproline Helix and Chignolin, regardless of predicting bias potential or force. Our model samples more realistic transition paths than the baselines with respect to the overall path and final conformation. We note that as the size of the molecule is larger, the EPD and EPCD performances decrease. For the large size of molecules including Chignolin, the bias potential produces better



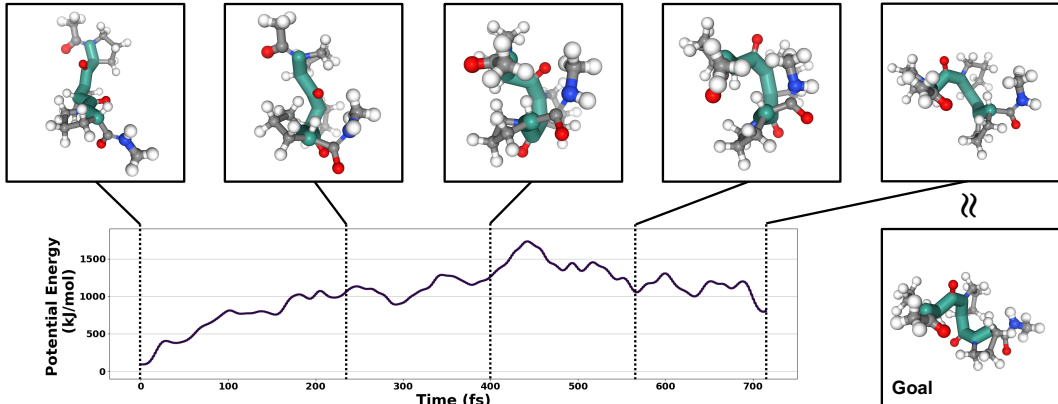


Figure 4: Visualization of a transition path from the meta-stable region PP-II to PP-I of Polyproline generated by our TPS-GFN. The top row visualizes the 3d view of states along the time horizon. The bottom row visualizes the potential energy along the time horizon. The backbone of the Polyproline is highlighted in green.

transition paths than bias force since the output of bias potential is always scalar regardless of the size of the molecule and the external force from the bias potential is conservative.

### 4.3 Qualitative results

In this section, we provide a qualitative comparison between our method and baselines and 3D visualizations. For Alanine Dipeptide, we show that our method generates diverse transition paths passing through both transition states. For Polyproline Helix and Chignolin, we visualize the transformation of molecular systems with their potential energy plot. For more visualization, please refer to [Appendix C](#), and [project page](#) for animation of the generated transition paths.

**Alanine Dipeptide.** In [Figure 3](#), we compare transition paths from our method to paths from baselines using the Ramachandran plot. We sample transition paths from  $C5$  to  $C7_{ax}$  which passes one of the two transition states in the energy landscape indicated by white stars in [Figure 3](#). In this experiment, we sampled 64 transition paths for all cases. The paths from unbiased MD simulations in [Figure 3a](#) remains trapped in the initial meta-stable region, and thus fail to produce transition paths. Both PIPS [14] and our TPS-GFN generates valid transition paths between  $C5$  and  $C7_{ax}$  as shown in [Figure 3b](#) and [Figure 3c](#), respectively. However, PIPS generates transition paths passing through only one of the transition states while our TPS-GFN generates diverse transition paths, passing through both transition states as shown in [Figure 3c](#).

**Polyproline Helix and Chignolin.** Since the CVs of the Polyproline Helix and the Chignolin are less understood, the Ramachandran plot is unavailable. Alternatively, we visualize the 3D views of the generated transition path at 5 different time steps with their potential energy along the time horizon. In [Figure 4](#), Our method successfully generates transition paths in terms of one CV candidate, handedness [44]. We observe change from the left-handed Helix to the right-handed Helix of the Polyproline and the potential plot which roughly increases up to approximately 440 fs and decreases after then. Similarly, in [Figure 5](#), our method captures the folding process of the Chignolin since the potential plot which roughly increases up to approximately 950 fs and decreases after then. We note that our method can produce various lengths of transition paths by cutting paths based on the relaxed indicator function. We also find the average time of the transition from PP-II to PP-I in Polyproline Helix is approximately 720 fs and the average folding time of chignolin is approximately 1000 fs.

## 5 Conclusion

In this work, we introduced a novel CV-free approach to sampling transition paths using generative flow networks (GFlowNets) to model bias potentials for efficient and diverse sampling. By reformulating the problem as amortized energy-based sampling and employing the one-step trajectory balance (TB) objective, our approach significantly improves the discovery of realistic transition paths compared to existing methods. Evaluations on proteins such as Alanine Dipeptide, Polyproline, and



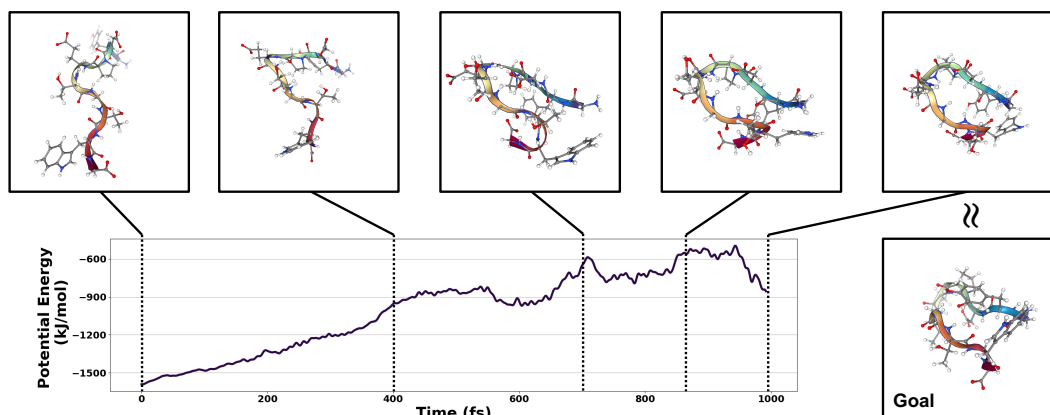


Figure 5: Visualization of a folding process of Chignolin generated by our TPS-GFN. The top row visualizes the 3d view of states along the time horizon. The bottom row visualizes the potential energy along the time horizon.

Chignolin demonstrate superior accuracy and diversity in identifying transition states. We believe that our works expand to more complex systems, with significant implications for drug discovery and material design.

**Limitation.** While our algorithm successfully samples transition paths for small peptides, we did not evaluate our algorithm for larger peptides or proteins due to the lack of computational budget. In addition, our work does not generalize across different pairs of meta-stable states or different molecular systems. This points to an interesting venue for future research, which would be more appealing for practical applications in drug discovery or material design.



## References

- [1] Evan Walter Clark Spotte-Smith, Ronald L Kam, Daniel Barter, Xiaowei Xie, Tingzheng Hou, Shyam Dwaraknath, Samuel M Blau, and Kristin A Persson. Toward a mechanistic model of solid–electrolyte interphase formation and evolution in lithium-ion batteries. *ACS Energy Letters*, 7(4):1446–1453, 2022.
- [2] Seihwan Ahn, Mannkyu Hong, Mahesh Sundararajan, Daniel H Ess, and Mu-Hyun Baik. Design and optimization of catalysts based on mechanistic insights derived from quantum chemical reaction modeling. *Chemical reviews*, 119(11):6509–6560, 2019.
- [3] Adrian J Mulholland. Modelling enzyme reaction mechanisms, specificity and catalysis. *Drug discovery today*, 10(20):1393–1402, 2005.
- [4] Stefano Piana, Kresten Lindorff-Larsen, and David E Shaw. Protein folding kinetics and thermodynamics from atomistic simulation. *Proceedings of the National Academy of Sciences*, 109(44):17845–17850, 2012.
- [5] Juyong Lee, In-Ho Lee, InSuk Joung, Jooyoung Lee, and Bernard R Brooks. Finding multiple reaction pathways via global optimization of action. *Nature Communications*, 8(1):15443, 2017.
- [6] Ron Elber. Perspective: Computer simulations of long time dynamics. *The Journal of chemical physics*, 144(6), 2016.
- [7] Philip Pechukas. Transition state theory. *Annual Review of Physical Chemistry*, 32(1):159–177, 1981.
- [8] Glenn M Torrie and John P Valleau. Nonphysical sampling distributions in monte carlo free-energy estimation: Umbrella sampling. *Journal of computational physics*, 23(2):187–199, 1977.
- [9] Giovanni Bussi and Davide Branduardi. Free-energy calculations with metadynamics: Theory and practice. *Reviews in Computational Chemistry Volume 28*, pages 1–49, 2015.
- [10] Jeffrey Comer, James C Gumbart, Jérôme Hénin, Tony Lelièvre, Andrew Pohorille, and Christophe Chipot. The adaptive biasing force method: Everything you always wanted to know but were afraid to ask. *The Journal of Physical Chemistry B*, 119(3):1129–1151, 2015.
- [11] Avishek Das, Dominic C Rose, Juan P Garrahan, and David T Limmer. Reinforcement learning of rare diffusive dynamics. *The Journal of Chemical Physics*, 155(13), 2021.
- [12] Tony Lelièvre, Geneviève Robin, Innas Sekkat, Gabriel Stoltz, and Gabriel Victorino Cardoso. Generative methods for sampling transition paths in molecular dynamics. *ESAIM: Proceedings and Surveys*, 73:238–256, 2023.
- [13] Magnus Petersen, Gemma Roig, and Roberto Covino. Dynamicsdiffusion: Generating and rare event sampling of molecular dynamic trajectories using diffusion models. 2023.
- [14] Lars Holdijk, Yuanqi Du, Ferry Hooft, Priyank Jaini, Berend Ensing, and Max Welling. Stochastic optimal control for collective variable free sampling of molecular transition paths. *Advances in Neural Information Processing Systems*, 36, 2024.
- [15] Emmanuel Bengio, Moksh Jain, Maksym Korablyov, Doina Precup, and Yoshua Bengio. Flow network based generative models for non-iterative diverse candidate generation. *Advances in Neural Information Processing Systems*, 34:27381–27394, 2021.
- [16] Yoshua Bengio, Salem Lahlou, Tristan Deleu, Edward J Hu, Mo Tiwari, and Emmanuel Bengio. Gflownet foundations. *Journal of Machine Learning Research*, 24(210):1–55, 2023.
- [17] Nikolay Malkin, Moksh Jain, Emmanuel Bengio, Chen Sun, and Yoshua Bengio. Trajectory balance: Improved credit assignment in gflownets. *Advances in Neural Information Processing Systems*, 35:5955–5967, 2022.



- [18] Jérôme Hénin, Tony Lelièvre, Michael R Shirts, Omar Valsson, and Lucie Delemotte. Enhanced sampling methods for molecular dynamics simulations [article v1. 0]. *Living Journal of Computational Molecular Science*, 4(1):1583–1583, 2022.
- [19] Fugao Wang and David P Landau. Efficient, multiple-range random walk algorithm to calculate the density of states. *Physical review letters*, 86(10):2050, 2001.
- [20] Christoph Dellago, Peter G Bolhuis, and David Chandler. Efficient transition path sampling: Application to lennard-jones cluster rearrangements. *The Journal of chemical physics*, 108(22):9236–9245, 1998.
- [21] Ernesto E Borrero and C Dellago. Avoiding traps in trajectory space: Metadynamics enhanced transition path sampling. *The European Physical Journal Special Topics*, 225:1609–1620, 2016.
- [22] Hendrik Jung, Roberto Covino, A Arjun, Christian Leitold, Christoph Dellago, Peter G Bolhuis, and Gerhard Hummer. Machine-guided path sampling to discover mechanisms of molecular self-organization. *Nature Computational Science*, 3(4):334–345, 2023.
- [23] Michael Plainer, Hannes Stark, Charlotte Bunne, and Stephan Günnemann. Transition path sampling with boltzmann generator-based mcmc moves. In *NeurIPS 2023 Generative AI and Biology (GenBio) Workshop*, 2023.
- [24] Sebastian Falkner, Alessandro Coretti, Salvatore Romano, Phillip Geissler, and Christoph Dellago. Conditioning normalizing flows for rare event sampling. *arXiv preprint arXiv:2207.14530*, 2022.
- [25] Luigi Bonati, GiovanniMaria Piccini, and Michele Parrinello. Deep learning the slow modes for rare events sampling. *Proceedings of the National Academy of Sciences*, 118(44):e2113533118, 2021.
- [26] Enrico Trizio and Michele Parrinello. From enhanced sampling to reaction profiles. *The Journal of Physical Chemistry Letters*, 12(35):8621–8626, 2021.
- [27] Dhiman Ray, Enrico Trizio, and Michele Parrinello. Deep learning collective variables from transition path ensemble. *The Journal of Chemical Physics*, 158(20), 2023.
- [28] Soojung Yang, Juno Nam, Johannes CB Dietschreit, and Rafael Gómez-Bombarelli. Learning collective variables for protein folding with labeled data augmentation through geodesic interpolation. *arXiv preprint arXiv:2402.01542*, 2024.
- [29] Jonathan Ho, Ajay Jain, and Pieter Abbeel. Denoising diffusion probabilistic models. *Advances in neural information processing systems*, 33:6840–6851, 2020.
- [30] Diederik P Kingma and Max Welling. Auto-encoding variational bayes. 2013.
- [31] Xinru Hua, Rasool Ahmad, Jose Blanchet, and Wei Cai. Accelerated sampling of rare events using a neural network bias potential. *arXiv preprint arXiv:2401.06936*, 2024.
- [32] Hilbert Johan Kappen and Hans Christian Ruiz. Adaptive importance sampling for control and inference. *Journal of Statistical Physics*, 162:1244–1266, 2016.
- [33] Alexandra Volokhova, Michał Koziarski, Alex Hernández-García, Cheng-Hao Liu, Santiago Miret, Pablo Lemos, Luca Thiede, Zichao Yan, Alán Aspuru-Guzik, and Yoshua Bengio. Towards equilibrium molecular conformation generation with gflownets. *arXiv preprint arXiv:2310.14782*, 2023.
- [34] Tony Shen, Mohit Pandey, and Martin Ester. TacoGFN: Target conditioned gflownet for structure-based drug design. 2023.
- [35] Alex Hernandez-Garcia, Alexandre Duval, Alexandra Volokhova, Yoshua Bengio, Divya Sharma, Pierre Luc Carrier, Michał Koziarski, and Victor Schmidt. Crystal-GFN: sampling crystals with desirable properties and constraints. In *37th Conference on Neural Information Processing Systems (NeurIPS 2023)-AI4MAI workshop*, 2023.



- [36] Moksh Jain, Emmanuel Bengio, Alex Hernandez-Garcia, Jarrid Rector-Brooks, Bonaventure FP Dossou, Chanakya Ajit Ekbote, Jie Fu, Tianyu Zhang, Michael Kilgour, Dinghuai Zhang, et al. Biological sequence design with gflownets. In *International Conference on Machine Learning*, pages 9786–9801. PMLR, 2022.
- [37] Nikolay Malkin, Salem Lahlou, Tristan Deleu, Xu Ji, Edward J Hu, Katie E Everett, Dinghuai Zhang, and Yoshua Bengio. Gflownets and variational inference. In *The Eleventh International Conference on Learning Representations*, 2022.
- [38] Giovanni Bussi and Michele Parrinello. Accurate sampling using langevin dynamics. *Physical Review E*, 75(5):056707, 2007.
- [39] Peter Eris Kloeden, Eckhard Platen, and Henri Schurz. *Numerical solution of SDE through computer experiments*. Springer Science & Business Media, 2012.
- [40] Volodymyr Mnih, Koray Kavukcuoglu, David Silver, Alex Graves, Ioannis Antonoglou, Daan Wierstra, and Martin Riedmiller. Playing atari with deep reinforcement learning, 2013.
- [41] Lorenz Richter, Ayman Boustati, Nikolas Nüsken, Francisco Ruiz, and Omer Deniz Akyildiz. Vargrad: a low-variance gradient estimator for variational inference. *Advances in Neural Information Processing Systems*, 33:13481–13492, 2020.
- [42] Tristan Deleu, Padideh Nouri, Nikolay Malkin, Doina Precup, and Yoshua Bengio. Discrete probabilistic inference as control in multi-path environments, 2024.
- [43] Chence Shi, Shitong Luo, Minkai Xu, and Jian Tang. Learning gradient fields for molecular conformation generation. In *International conference on machine learning*, pages 9558–9568. PMLR, 2021.
- [44] Mahmoud Moradi, Volodymyr Babin, Christopher Roland, Thomas A Darden, and Celeste Sagui. Conformations and free energy landscapes of polypyrrolone peptides. *Proceedings of the National Academy of Sciences*, 106(49):20746–20751, 2009.
- [45] Salem Lahlou, Tristan Deleu, Pablo Lemos, Dinghuai Zhang, Alexandra Volokhova, Alex Hernández-Garcia, Léna Néhale Ezzine, Yoshua Bengio, and Nikolay Malkin. A theory of continuous generative flow networks. In *International Conference on Machine Learning*, pages 18269–18300. PMLR, 2023.
- [46] Peter Eastman, Raimondas Galvelis, Raúl P Peláez, Charles RA Abreu, Stephen E Farr, Emilio Gallicchio, Anton Gorenko, Michael M Henry, Frank Hu, Jing Huang, et al. Openmm 8: Molecular dynamics simulation with machine learning potentials. *The Journal of Physical Chemistry B*, 128(1):109–116, 2023.
- [47] Adam Paszke, Sam Gross, Francisco Massa, Adam Lerer, James Bradbury, Gregory Chanan, Trevor Killeen, Zeming Lin, Natalia Gimelshein, Luca Antiga, et al. Pytorch: An imperative style, high-performance deep learning library. *Advances in neural information processing systems*, 32, 2019.
- [48] Matthias Rupp, Alexandre Tkatchenko, Klaus-Robert Müller, and O Anatole Von Lilienfeld. Fast and accurate modeling of molecular atomization energies with machine learning. *Physical review letters*, 108(5):058301, 2012.



## A Generative Flow Networks

In this section, we briefly introduce the concept of GFlowNets and explain how we derive Equation (2). We refer to Lahlou et al. [45] for a comprehensive study on formalizing GFlowNets on continuous state spaces.

**Generative flow networks.** GFlowNet [15, 16] is a framework to sequentially construct samples  $s \in \mathcal{S}$  proportional to a reward function  $R(s)$ , where  $\mathcal{S}$  is a set of data. In other words, GFlowNet aims to learn a target distribution  $p^*(s)$  defined as:

$$p^*(s) = \frac{R(s)}{Z}, \quad Z = \int_{\mathcal{S}} R(s) ds,$$

where  $Z$  is the normalizing constant. To this end, GFlowNet samples a trajectory  $\tau = (s_0, \dots, s_L) \in \{s_0\} \times \mathcal{S}^L$  of length  $L$  through a series of state transitions made by a forward policy  $P_F(s_l|s_{l-1}; \theta)$  for  $l = 1, \dots, L$ , where  $s_0$  is the fixed initial state of all trajectories and  $s = s_L$  is the terminal state we want to sample.

**Flow matching.** To train the forward policy, GFlowNet introduces an auxiliary backward policy  $P_B(s_{l-1}|s_l; \theta)$  and matches the *forward flow*  $Z_\theta P_F(\tau; \theta)$  with *backward flow*  $R(s)P_B(\tau|s; \theta)$  using the *flow matching* objective over the trajectories  $\tau = (s_0, \dots, s_L)$ :

$$Z_\theta \prod_{l=1}^L P_F(s_l|s_{l-1}; \theta) \approx R(s) \prod_{l=1}^L P_B(s_{l-1}|s_l; \theta) \quad (4)$$

where  $Z_\theta \in \mathbb{R}$  is a learnable scalar parameter to estimate the normalization constant  $Z$ . Equation (4) induces  $Z_\theta P_F(s) \approx R(s)$ , by marginalizing forward and backward flows over set of trajectories  $\mathcal{T}(s)$  ending at the terminal state  $s$ , i.e.,  $\int_{\tau \in \mathcal{T}(s)} Z_\theta P_F(\tau; \theta) d\tau = Z_\theta P_F(s)$  and  $\int_{\tau \in \mathcal{T}(s)} R(s) P_B(\tau|s; \theta) d\tau = R(s)$ . In other words, we can sequentially construct a sample  $s$  proportional to a reward function  $R(s)$  through a series of state transitions by the forward policy after minimizing the flow matching objective.

**Trajectory balance.** For flow matching, Malkin et al. [17] proposed the trajectory balance objective:

$$\mathcal{L}_{\text{TB}}(s_1, \dots, s_L; \theta) = \left( \log \frac{Z_\theta \prod_{l=1}^L P_F(s_l|s_{l-1}; \theta)}{R(s_L) \prod_{l=1}^L P_B(s_{l-1}|s_l; \theta)} \right)^2,$$

which corresponds to minimizing the squared difference of logarithms on the left and right-hand side of Equation (4). In particular, one-step GFlowNets, i.e.,  $L = 1$ , induces the following training objective:

$$\mathcal{L}_{\text{TB}}(s_1; \theta) = \left( \log \frac{Z_\theta P_F(s_1|s_0; \theta)}{R(s_1)} \right)^2, \quad (5)$$

where  $P_B(s_0|s_1; \theta)$  is ignored since  $s_0$  is the constant initial state. Note that the detailed balance [16] objective also reduces to the same formula as in Equation (5) with one-step GFlowNets.

**Transition path sampling via GFlowNets.** In this work, we formulate the transition path sampling problem (Equation (1)) as one-step GFlowNets. We set  $\mathcal{S}$  as a set of paths  $\mathbf{x}_{1:T}$  of length  $T$  starting at the initial state  $s_0 = \mathbf{x}_0$  and the reward function as

$$R(\mathbf{x}_{1:T}) = \mathbf{1}_B(\mathbf{r}_T) \prod_{t=1}^T p_{\text{MD}}(\mathbf{x}_t|\mathbf{x}_{t-1}) \propto p_{\mathcal{A}, \mathcal{B}}(\mathbf{x}_{1:T}|\mathbf{x}_0). \quad (6)$$

Since  $P_F(s_1|s_0; \theta) = p_\theta(\mathbf{x}_{1:T}|\mathbf{x}_0)$ , one can derive Equation (2) from Equation (5):

$$\mathcal{L}(\mathbf{x}_{1:T}; \theta) = \left( \log \frac{Z_\theta \prod_{t=1}^T p_\theta(\mathbf{x}_t|\mathbf{x}_{t-1})}{\mathbf{1}_B(\mathbf{r}_T) \prod_{t=1}^T p_{\text{MD}}(\mathbf{x}_t|\mathbf{x}_{t-1})} \right)^2.$$



## B Experiment details

We implement codes based on OpenMM [46] and Pytorch [47] libraries, and run codes on a single GPU (NVIDIA RTX 3090 or RTX A5000).

### B.1 OpenMM configurations

We run MD simulations to sample paths and evaluate them at the temperature of 300K, using the Langevin integrator. Other configurations depend on molecules as shown in Table 3.

Table 3: OpenMM configurations depending on molecules.

Molecule	Time horizon	Time step	Force field	Solvent
Alanine Dipeptide	500 fs	1 fs	amber99sbildn	tip3p
Polyproline Helix	10000 fs	2 fs	amber/protein.ff14SBonlysc	implicit/gbn2
Chignolin	5000 fs	1 fs	amber/protein.ff14SBonlysc	implicit/gbn2

### B.2 Model configurations

We report the model configurations used to produce the results from PIPS [14] and TPS-GFN in Table 4 and Table 5, respectively.

Table 4: Model configurations used to produce the results from PIPS.

Molecule	Rollout	LR	Samples	Brownian motion std
Alanine Dipeptide	15000	$10^{-5}$	16	0.1
Polyproline Helix	500	$3 \times 10^{-5}$	25	0.1
Chignolin	500	$10^{-4}$	16	0.05

Table 5: Model configurations used to produce the results from TPS-GFN.

Molecule	Force	Flexible	Rollout	Trains per rollout	LR	Log Z LR	Samples	Target std( $\sigma$ )
Alanine Dipeptide	✗	✗	10000	2000	0.01	0.001	16	0.05
Alanine Dipeptide	✓	✗	10000	2000	0.01	0.001	16	0.05
Polyproline Helix	✗	✓	5000	200	0.0001	0.01	2	0.2
Polyproline Helix	✓	✓	5000	200	0.001	0.01	2	0.2
Chignolin	✗	✓	5000	200	0.0001	0.01	2	0.2
Chignolin	✓	✓	5000	200	0.0001	0.01	2	0.2

For Alanine Dipeptide, we remove the flexibility of length in our method by replacing our relaxed indicator function  $\hat{\mathbf{1}}_{\mathcal{B}}(\mathbf{x}_{1:T})$  with  $\hat{\mathbf{1}}_{\mathcal{B}}(\mathbf{x}_T) = \exp(-\|D(\mathbf{r}_T) - D(\mathbf{r}_{\mathcal{B}})\|_F^2/2\sigma^2)$  which slightly increases performance. However, other molecules benefit from flexibility.

### B.3 Evaluation metrics

Following the prior work [14], we adopt three metrics for evaluation: (i) Expected pairwise distance (EPD), (ii) Target hit percentage (THP), and (iii) Energy transition point (ETP).

**Expected pairwise distance (EPD).** The interatomic pairwise distance matrix  $D(\cdot)$  [43] expresses molecular conformation in an E(3)-invariant manner. EPD measures the similarity between the final conformation  $\mathbf{r}_t$  and the target conformation  $\mathbf{r}_{\mathcal{B}}$  by calculating the square distance between interatomic pairwise distance matrices defined as follows:

$$\text{EPD}(\mathbf{r}_t, \mathbf{r}_{\mathcal{B}}) = \frac{1}{N^2} \|D(\mathbf{r}_t) - D(\mathbf{r}_{\mathcal{B}})\|_F^2$$

Where  $t$  is the index of the final conformation of transition paths.



**Target hit percentage (THP).** While EPD continuously measures the distance from the fixed target conformation, THP measures the success of paths arriving at the target meta-stable state  $\mathcal{B}$  in a binary manner. For the final conformations  $\{r^{(i)}\}_{i=1}^M$  of  $M$  paths, THP is defined as follows:

$$\text{THP} = \frac{|\{i : r^{(i)} \in \mathcal{B}\}|}{M}$$

For the alanine dipeptide, we use  $\mathcal{B} = \{r : |\phi(r) - \phi(r_{\mathcal{B}})| + |\psi(r) - \psi(r_{\mathcal{B}})| < 0.75\}$  where  $(\phi, \psi)$  is the collective variable consisting of two torsion angles.

**Energy transition point (ETP).** Unlike EPD and THP which evaluate the final conformation of a transition path, ETP measures the ability of the method to find the transition states when crossing the energy barrier. ETP refers to the maximum potential energy among states in a transition path. Formally, given a transition path  $\mathbf{x}_{0:t}$  that reaches the target meta-stable region i.e.,  $\mathbf{r}_t \in \mathcal{B}$ , ETP computes

$$\text{ETP}(\mathbf{x}_{0:t}) = \max_{i \in [0, t]} U(\mathbf{r}_i)$$

However, we point out that these metrics can not measure the realism of the paths with respect to unbiased molecular dynamics. Thus, we propose metrics for the realism of paths and final conformations. The likelihood of the unbiased molecular dynamics is a part of the target distribution  $p_{\mathcal{A}, \mathcal{B}}(\mathbf{x}_{1:T} | \mathbf{x}_0)$  which explains how realistic the sampled transition paths are.

**Log Likelihood (LL).** Log Likelihood (LL) refers to the log-likelihood of unbiased molecular dynamics as follows:

$$\text{LL}(\mathbf{x}_{0:T}) = \frac{1}{T} \sum_{t=1}^T \log p_{\text{MD}}(\mathbf{x}_t | \mathbf{x}_{t-1})$$

We divide by  $T$  to evaluate paths regardless of length. For the realism of final conformations, we focus on the potential energy of them. We propose two metrics, potential Energy of the Final Point (EFP) and Expected Pairwise Coulomb Distance (EPCD).

**Potential energy of final point (EFP).** The final conformation of a transition path from unbiased molecular dynamics should have low potential energy due to meta-stability. EFP measures the potential  $U(r_t)$  of the final conformation of a transition path sampled from the model.

**Expected pairwise coulomb distance (EPCD).** Coulomb matrix [48]  $C(r)$  of the final conformation  $r$  describes electrostatic interaction between nuclei in the final conformation  $r$  and is formulated as follows:

$$C(r)_{ij} = \begin{cases} 0.5Z_i^{2.4} & \text{for } i = j \\ Z_i Z_j / \|r_i - r_j\| & \text{for } i \neq j \end{cases}$$

where  $Z_i$  and  $Z_j$  are the atomic numbers and  $r_i, r_j$  are the positions of atoms  $i$  and  $j$ , respectively. The atomic numbers  $Z_i$  and  $Z_j$  of the Coulomb matrix reflect atomic mass and energy level around the final conformation better than the distance matrix. We propose EPCD which replaces the distance metrics used in EPD with the Coulomb matrix and is defined as follows:

$$\text{EPCD}(\mathbf{r}_t, \mathbf{r}_{\mathcal{B}}) = \frac{1}{N^2} \|C(\mathbf{r}_t) - C(\mathbf{r}_{\mathcal{B}})\|_F^2$$

EPCD measures both geometric and electrostatic similarities between the final conformation  $\mathbf{r}_t$  and the target conformation  $\mathbf{r}_{\mathcal{B}}$ .

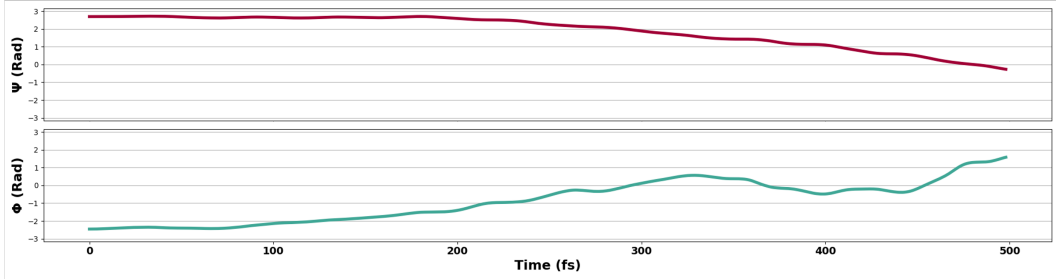


## C Additional visualizations

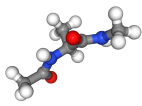
In this section, we provide additional visualizations of transition paths for each molecular system, generated by our TPS-GFN.

### C.1 Alanine Dipeptide

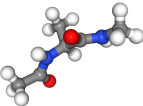
In Figure 6, we visualize a collective variable (CV), i.e., two dihedral angles ( $\phi, \psi$ ) along the time horizon and 3D views of a transition path from the meta-stable region  $C5$  to  $C7_{ax}$  with the target conformation  $r_{C7_{ax}}$ . Our model successfully generates a transition path since the final frame in Figure 6l is in  $C7_{ax}$ .



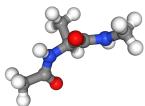
(a) Visualization of  $\psi$  and  $\phi$  along the time horizon



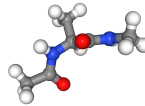
(b) Frame 0 ( $= r_{C5}$ )



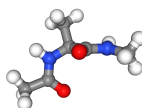
(c) Frame 50



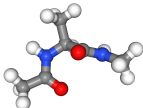
(d) Frame 100



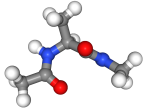
(e) Frame 150



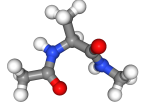
(f) Frame 200



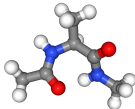
(g) Frame 250



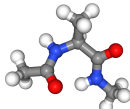
(h) Frame 300



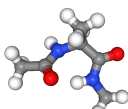
(i) Frame 350



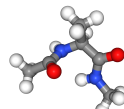
(j) Frame 400



(k) Frame 450



(l) Frame 498



(m)  $r_{C7_{ax}}$

Figure 6: 3D view of a transition path from the meta-stable region  $C5$  to  $C7_{ax}$  with the target conformation  $r_{C7_{ax}}$



## C.2 Polyproline Helix

In Figure 7, we visualize 3D views of a transition path from the meta-stable region PP-II to PP-I.

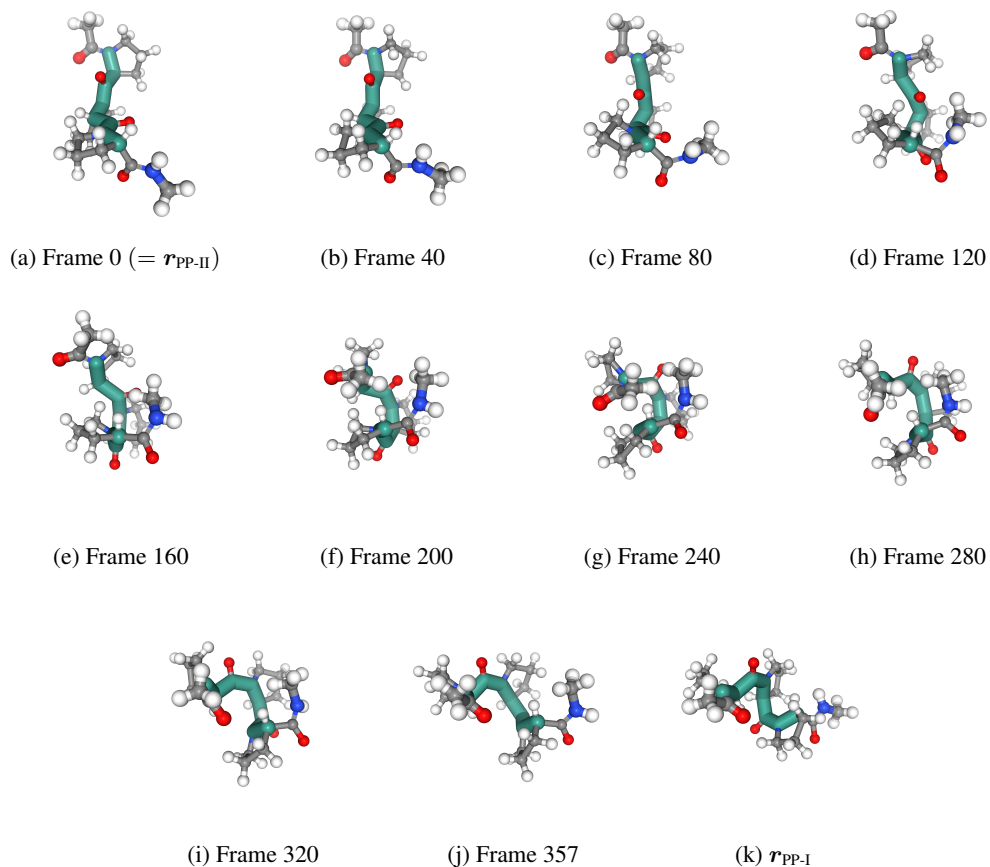


Figure 7: 3D view of a transition path from the meta-stable region PP-II to PP-I with the target conformation  $r_{\text{PP-I}}$



### C.3 Chignolin

In Figure 8, we visualize 3D views of a Chignolin folding process.

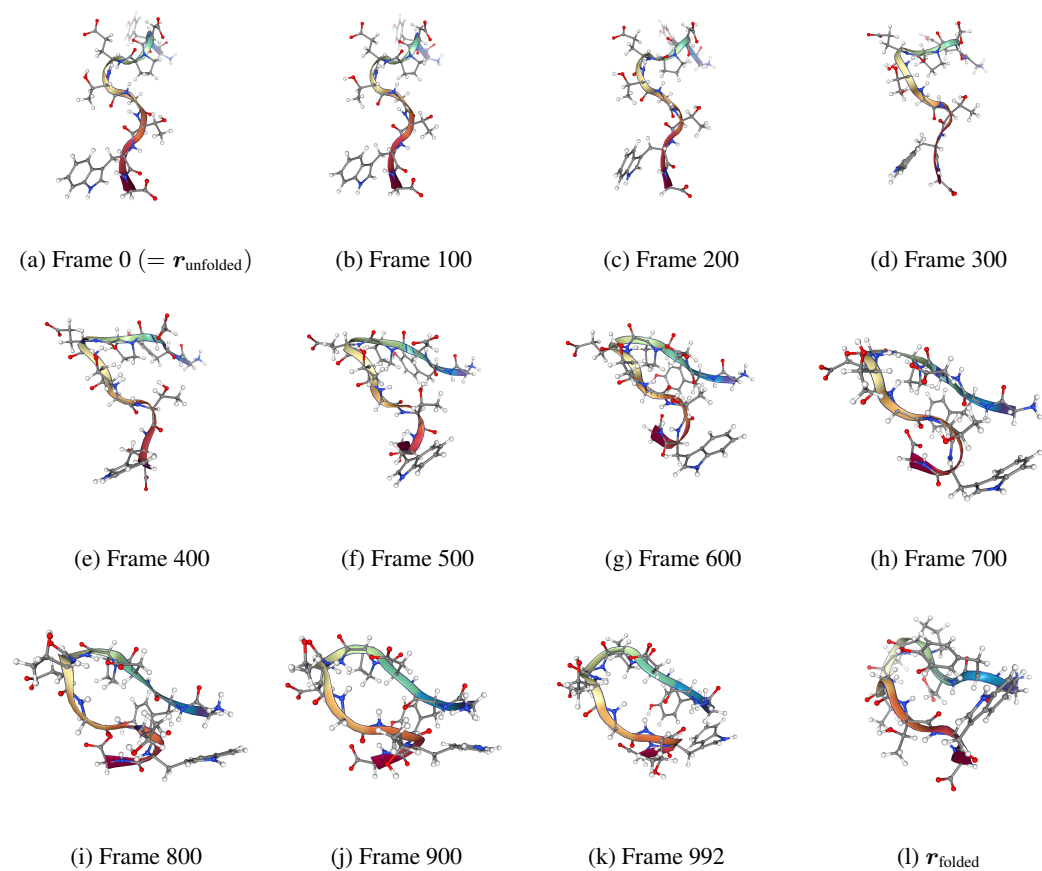


Figure 8: 3D visualization of a Chignolin folding process with the target conformation  $\mathbf{r}_{\text{folded}}$